The Canadian Mineralogist
Vol. 44, pp. 189-206 (2006)

INTERPRETATION OF SELECTED STRUCTURES OF THE BISMUTHINITE – AIKINITE SERIES AS COMMENSURATELY MODULATED STRUCTURES

VACLAV PETŘÍČEK

Physics Institute, Czech Academy of Sciences, Na Slovance 2, CZ–180 40 Prague 8, Czech Republic

EMIL MAKOVICKY[§]

Geological Institute, University of Copenhagen, Øster Voldgade 10, DK–1350 Copenhagen K, Denmark

ABSTRACT

The bismuthinite – aikinite (Bi_2S_3 – $CuPbBiS_3$) series of ordered derivatives (superstructures) is based on the incremental Bi + vacancy ⟶ Pb + Cu substitution. Selected structures of this series, gladite, salzburgite, paarite and krupkaite, were refined as commensurately modulated structures using the superspace approach. The superspace group *Pmcn*(0β0)00*s* was used for all these structures, β assuming the value of 1/3, 1/4, 1/5, and 2 in the above order. Two independent large-cation positions, one Cu position (in oversubstituted members, two) and three S positions were refined for the sequence of one or three to five subcells forming the above structures using the summation of sinusoidal functions for positional and displacement parameters. In this paper, we describe, in terms intended for non-specialists, our choice of the superspace group, its application to individual superstructures, the details of the structure refinement, and the structural interpretation of the results.

Keywords: bismuthinite – aikinite series, gladite, salzburgite, paarite, krupkaite, superspace approach, commensurately modulated structures.

SOMMAIRE

La série bismuthinite – aikinite (Bi_2S_3 – $CuPbBiS_3$) de dérivés ordonnés (surstructures) est fondée sur la substitution par incréments de Bi + lacune ⟶ Pb + Cu. Nous avons affiné la structure de certains membres de cette série, dont gladite, salzburgite, paarite et krupkaïte, en les traitant de structures à modulations commensurables en termes de surespace. Le groupe de surespace *Pmcn*(0β0)00*s* a été utilisé pour toutes ces structures, β prenant une valeur de1/3, 1/4, 1/5, et 2 dans ces minéraux, respectivement. Deux positions indépendantes occupées par de gros cations, le Cu dans une (deux dans les membres sursubstitués), et trois positions occupées par le S ont été affinées pour la séquence de une ou trois à cinq sous-mailles formant ces structures en utilisant les fonctions sinusoïdales des paramètres de position et de déplacement. Dans ce travail, nous décrivons, en termes convenables pour les non-spécialistes, notre choix du groupe de surespace, son application aux surstructures individuelles, les détails de l'affinement de la structure, et l'interprétation structurale des résultats.

(Traduit par la Rédaction)

Mots-clés: série bismuthinite – aikinite, gladite, salzburgite, paarite, krupkaïte, concept de surespace, structures à modulations commensurables.

§ *E-mail address*: emilm@geol.ku.dk

Introduction

The bismuthinite – aikinite series (Bi_2S_3 – $CuPbBiS_3$) is one of the classical series of sulfosalts. This series of ordered derivatives $Cu_xPb_xBi_{2-x}S_3$ has been a subject of long and intense research about the textural, compositional and structural aspects (Ohmasa & Nowacki 1970a, b, Kohatsu & Wuensch 1971, 1976, Syneček & Hybler 1974, Mumme 1975, Horiuchi & Wuensch 1976, 1977, Harris & Chen 1976, Mumme & Watts 1976, Mumme *et al*. 1976, Chen *et al*. 1978, Makovicky & Makovicky 1978, Žák 1980, Pring 1989, 1995, Mozgova *et al*. 1990, Balić-Žunić *et al*. 2002, Topa *et al*. 2002). The most recent of these investigations focused on descriptions of three new crystal structures, among which are two four-fold derivatives, salzburgite, $Cu_{1.6}Pb_{1.6}Bi_{6.4}S_{12}$ (Topa *et al*. 2000), and emilite, $Cu_{2.7}Pb_{2.7}Bi_{5.3}S_{12}$ (Balić-Žunić *et al*. 2002) and a new five-fold derivative, paarite, $Cu_{1.7}Pb_{1.7}Bi_{6.3}S_{12}$ (Makovicky *et al*. 2001). This enlargement of the bismuthinite–aikinite series establishes it as a series of one-, three-, four-, and five-fold superstructures built by compositional and positional modification of the basic Bi_2S_3 structure. An attempt to give an alternative, unified description of these superstructures for the gladite $CuPbBi_5S_9$ – krupkaite $CuPbBi_3S_6$ range as commensurately modulated structures by means of the superspace approach is the topic of the present contribution. The rationale of this study was to find out how closely and how clearly the local and the global features of this structural series are reflected in the results of this novel approach. We attempt to describe the basis and the procedures of the superspace refinement in terms that are clear to the non-specialist.

The Bismuthinite – Aikinite Series

Bismuthinite – aikinite derivatives are superstructures of the structure of bismuthinite, Bi_2S_3, formed by incremental substitution of bismuth in one of the two Bi sites by lead, connected with gradual filling of the adjacent, void coordination tetrahedron by Cu, in agreement with the scheme Bi + □ → Pb + Cu. In a classical description, these structures are composed of M_4S_6 ribbons with metal atoms in two distinct positions (Fig. 1). The *M*2 sites (Bi2 in bismuthinite) are centrally situated in the ribbon; both Bi and Pb occur in them. The terminal Bi1 sites accept only bismuth. Both are in square pyramidal coordination M_{3+2} that can be completed to monocapped prismatic by adding two sulfur atoms from the adjacent ribbon(s). The tetrahedral voids are situated in the inter-ribbon space; they flank each ribbon at its terminal portions, and are sandwiched between *M*1 and *M*2 coordination prisms of an adjacent ribbon. Lone-electron pairs in Bi (and Pb) are oriented away from the ribbon surfaces, into the inter-ribbon space.

The step-wise replacement of Bi + vacancy by Pb + Cu leads in the ordered derivatives (*i.e.,* at ambient temperature) to three distinct types of ribbons (Ohmasa & Nowacki 1970a): "bismuthinite-like" ribbons Bi_4S_6 with an adjacent tetrahedral void, "krupkaite-like" ribbons $CuPbBi_3S_6$ with one of the two *M*2 sites containing Pb and the adjacent tetrahedral void filled by Cu, and "aikinite-like" ribbons $Cu_2Pb_2Bi_2S_6$ in which both *M*2 sites are occupied by Pb and both adjacent tetrahedral voids are filled by Cu (Fig. 2). Partial replacement of Bi2 by Pb, associated with partial occupancy of adjacent tetrahedra by Cu, has been found in several of these phases (*e.g.,* Topa *et al*. 2000, Makovicky *et al*. 2001, Balić-Žunić *et al*. 2002). All these structures share a common 11.4 Å subcell, which is the unit cell of the underlying Bi_2S_3-like substructure. It will be of considerable importance in the derivations that follow. The superstructure building occurs along [010], yielding the 1*b*, 3*b*, 4*b* and 5*b* superstructures. These are invariably ordered arrangements of two out of the three types of ribbon mentioned above.

An alternative description, in form of structure intervals (modules) between adjacent planes (010) of fully occupied copper tetrahedra, was put forward in the three above-mentioned latest works as well. The known intervals are those from gladite (1½ $b_{subcell}$ wide), krupkaite (1$b_{subcell}$ wide) and aikinite (½ $b_{subcell}$ wide). The more complicated, intermediate phases are then combinations of these modules, *e.g.,* salzburgite is a sequence of two gladite-like and one krupkaite-like modules. This system of modules is not equivalent to the model of commensurate modulation described in this paper.

Choice of Superspace Group

The principal aim of the current investigation was to find and apply a single (3 + 1)-dimensional superspace group to as many superstructures as possible (preferably all) of the bismuthinite – aikinite series. The (3 + 1)-dimensional superspace groups, as introduced by deWolff *et al*. (1981), are four-dimensional symmetry groups in which three dimensions correspond to the classical three-dimensional space, and are used here to describe the basic (sub)structure. The fourth dimension is used in the current type of problems for description of the periodic wave-modulation of this basic structure. The usual approach, in reciprocal space, relates the vectors **a***, **b*** and **c*** to the reciprocal lattice of the main reflections (*i.e.,* the Fourier transform of the basic unmodulated structure), whereas **q** is the wave-vector of the modulation. The corresponding Miller indices are usually denoted as *h*, *k*, *l* and *m* (International Tables, volume C). The symbol of a superspace group consists of three parts: (a) the space group of the basic structure (substructure) (International Tables, volume A), (b) the definition of the modulation vector **q** in terms of recip-

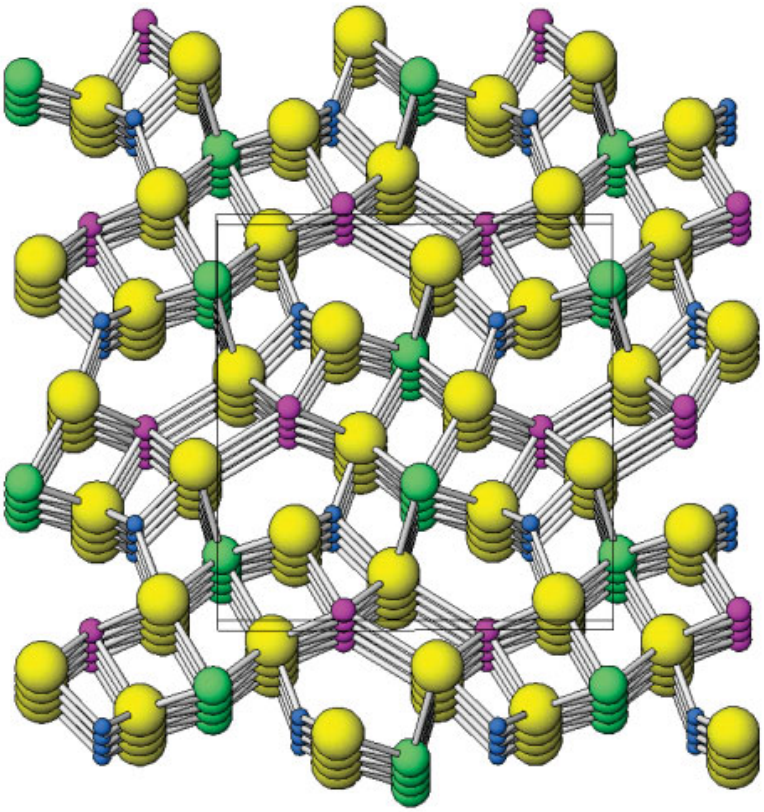

FIG. 1. The crystal structure of aikinite $CuPbBiS_3$ (Kohatsu & Wuensch 1971). Positions *M*1 are occupied by Bi, *M*2 by Pb, and all tetrahedral voids are occupied by Cu. Atoms are situated at two distinct heights, 2 Å apart.

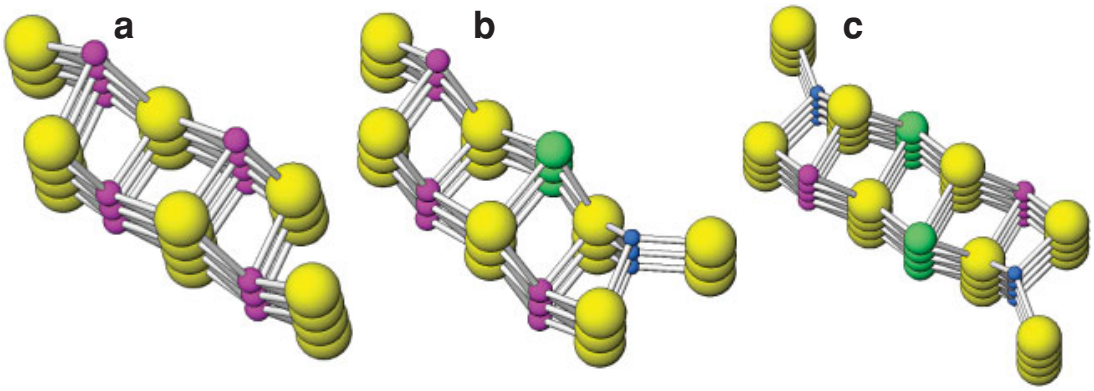

FIG. 2. Bismuthinite-like ribbons Bi_4S_6, krupkaite-like ribbons $CuPbBi_3S_6$, and aikinite-like ribbons $Cu_2Pb_2Bi_2S_6$, from the crystal structures of the bismuthinite – aikinite series.

rocal-space parameters, $\mathbf{q} = \alpha\mathbf{a}^* + \beta\mathbf{b}^* + \gamma\mathbf{c}^*$ so that the bracketed values in the superspace-group symbol are $\sigma = (\alpha,\beta,\gamma)$ [in this expression, the components of the modulation vector, restricted by symmetry to a special fraction, are written explicitly, others by the corresponding Greek symbols α, β or γ], and (c) the

translational parts, along the fourth dimension, of the symmetry operators of the space group indicated in part (a). Each symbol is one of the letters 0, s, t, q or h according to the rules described in International Tables volume C, *e.g.,* s = 1/2, and t = ±1/3.

Gladite, a three-fold superstructure, was taken as a point of departure. The choice of the supergroup was based on the symmetry of the diffraction pattern and the observed systematic extinctions. The symmetry of the substructure is *Pmcn*. In terms of the complete, 33 Å gladite lattice, the reflections are $\mathbf{Q} = H\mathbf{A}^* + K\mathbf{B}^* + L\mathbf{C}^*$. Rewritten in terms of a 1**b** subcell plus satellites, $\mathbf{Q} = h\mathbf{a}^* + k\mathbf{b}^* + l\mathbf{c}^* + m\mathbf{q}$, where $\mathbf{q} = \mathbf{B}^* = \mathbf{b}^*/3$. Thus the main (*i.e.,* subcell) reflections have $K = 3k$, and the satellites become $K = 3k + m$ for $m = 1$ or -1. The first condition for reflection following from the presence of a *c* glide plane along **B** in a form *H*0*L*: $L = 2n$ affects only reflections for which $K = 3k + m = 0$, and therefore it is equivalent in the superspace description to h0*l*0: $l = 2n$. The second condition for reflection for *HK*0: $H + K = 2n$ (*i.e.,* the *n* glide plane), turns into *hk*0*m*: $h+3k+m = 2n$ in the superspace description, which can be simplified to $h + k + m = 2n$.

The reflection conditions as derived above lead to the superspace group *Pmcn* (0β0)00*s*. The value of β for the three-fold structure is equal 1/3. The letter *s* in the part (c) of the symbol of the superspace group means that the glide mirror *n* along **c** has the translation component along "internal", *i.e.,* the fourth direction equal to 1/2.

In the following, we shall show how the matrix form of all symmetry operators can be derived from the superspace group-symbol and how they can be used to derive four-dimensional reflection conditions. The general symmetry-operator is represented by 4 × 4 rotation matrix combined with a four-dimensional translation vector.

$$\left(\mathbf{R}, \mathbf{t}\right) = \left[\begin{array}{cc|c} \mathbf{R}_E & 0 & \mathbf{t}_E \\ \mathbf{R}_M & \mathbf{R}_I & \mathbf{t}_I \end{array}\right]$$

In this matrix, $\mathbf{R}_E$, $\mathbf{R}_M$ and $\mathbf{R}_I$ are, respectively, 3 × 3 external, 1 × 3 mixed and 1 × 1 internal part of the rotation matrix, and $\mathbf{t}_E$ and $\mathbf{t}_I$ are, respectively, external and internal translation vectors. "External" refers in the jargon of modulation crystallography to the physical three-dimensional space, whereas "internal" refers to the additional, fourth coordinate (also referred to as the "complementary" or "perpendicular" space). From the way the superspace was introduced, it follows also that the right upper part of the rotation matrix is identically equal to zero, and that the remaining parts of the rotation matrix are related by the equation $\mathbf{q} = \mathbf{R}_E \cdot \mathbf{R}_I \bullet \mathbf{q} = \mathbf{R}_M$. The $\mathbf{R}_M$ part is equal to zero for our case [for more details, see deWolff *et al*. (1981)], and thus all the rotation matrices are reduced to two blocks composed of $\mathbf{R}_E$, $\mathbf{R}_I$. The external rotation-matrix and translation vectors can be determined from the three-dimensional space-group symbol, part (a) as for three-dimensional space groups. The internal rotation part is equal to +1 if $\mathbf{R}_E$ transforms the **q** vector into itself, and –1 if it transforms this vector to **–q**. The internal translation part $\mathbf{t}_I$ is derived from part (c), as mentioned above.

In (3 + 1)-dimensional space, the first operation, *m*, has the rotational matrix $\mathbf{R}_E$ and the translation vector $\mathbf{t}_E$ as follows:

$$\left(\mathbf{R}_\mathrm{m} \mid \mathbf{t}_\mathrm{m}\right) = \left[\begin{array}{cccc|c} -1 & 0 & 0 & 0 & 1/2 \\ 0 & 1 & 0 & 0 & 0 \\ 0 & 0 & 1 & 0 & 0 \\ 0 & 0 & 0 & 1 & 0 \end{array}\right]$$

The value of 1 for the (1 × 1) $\mathbf{R}_I$ of the 4 × 4 $\mathbf{R}_\mathrm{m}$ matrix suggests that *m* does not reverse the sense of the modulation vector **q** (see above).

For the *c* glide plane,

$$\left(\mathbf{R}_\mathrm{c} \mid \mathbf{t}_\mathrm{c}\right) = \left[\begin{array}{cccc|c} 1 & 0 & 0 & 0 & 0 \\ 0 & -1 & 0 & 0 & 1/2 \\ 0 & 0 & 1 & 0 & 1/2 \\ 0 & 0 & 0 & -1 & x \end{array}\right]$$

The $\mathbf{R}_I$ value is –1 in this case (*c* reverses the sense of the **q** vector). The parameter *x* cannot be directly derived from the symbol, and it will be deduced from the combination of other symmetry elements later.

The transformation matrix of the *n* glide plane is

$$\left(\mathbf{R}_\mathrm{n} \mid \mathbf{t}_\mathrm{n}\right) = \left[\begin{array}{cccc|c} 1 & 0 & 0 & 0 & 1/2 \\ 0 & 1 & 0 & 0 & 1/2 \\ 0 & 0 & -1 & 0 & 1/2 \\ 0 & 0 & 0 & 1 & 1/2 \end{array}\right]$$

We combine it with m in order to define the two-fold rotation operation $m \times n = 2$, which we further combine with inversion in order to obtain $2 \times \bar{1} = c$. This allows us to conclude that the parameter x is equal to ½.

For the reflections invariant with respect to the rotation part of the operator in question, the translation vectors can be used to derive reflection conditions by means of the scalar product **H** • **t** = integer. Thus,

$$\begin{pmatrix} 0 & k & l & m \end{pmatrix} \circ \begin{pmatrix} 1/2 \\ 0 \\ 0 \\ 0 \end{pmatrix} = 0$$

i.e., no extinctions are produced by the mirror plane m

$$\begin{pmatrix} h & 0 & l & 0 \end{pmatrix} \circ \begin{pmatrix} 0 \\ 1/2 \\ 1/2 \\ 1/2 \end{pmatrix} = n$$

i.e., for ($h0l0$): $l = 2n$ only because of the c glide plane, and

$$\begin{pmatrix} h & k & 0 & m \end{pmatrix} \circ \begin{pmatrix} 1/2 \\ 1/2 \\ 1/2 \\ 1/2 \end{pmatrix} = n$$

i.e., for ($hk0m$): $h + k + m = 2n$ because of the n glide plane, as already derived above. Analogous schemes are valid for the five-fold superstructure.

In this derivation, we ignored the fact that for these commensurate structures, any reflection (h,k,l,m) can be alternatively understood as all reflections fulfilling the condition (h,$k + n$,l,$m - 3n$) for the three-fold superstructure (*i.e.,* a first-order satellite of one main reflection overlaps with the second-order satellite of the adjacent main reflection, *etc.*) and the condition (h,$k + n$,l,$m - 5n$) for the five-fold superstructure. All these reflections obey the same condition for reflection, ($hk0m$): $h + k + m = 2n$. For the four-fold superstructure (*i.e.,* salzburgite), the above rules give problems; reflections (h,$k + n$,l,$m - 4n$) lead to a different parity for the reflection conditions where n is even and where n is odd. The diffraction spot should thus be present according to the first (even) representation, and it should be absent according to the second (odd) representation. The symmetry element that leads to such an inconsistency cannot be present in the superstructure.

The superspace approach to modulated structures leads to translational symmetry in (3 + 1)-dimensional direct space. The unit cell is now (3 + 1)-dimensional, and the atom parameters are described by modulation functions defined within this unit cell and not by discrete values as it was in the three-dimensional space. The real three-dimensional structure can be derived as a section through (3 + 1)-dimensional superspace perpendicular to the x_4 axis (Fig. 3a). There are an infinite number of such sections, each characterized by the value of x_4 at the intersection of the hyperplane with the x_4 axis. The coordinate t that fulfills the following condition (see Fig. 3a), $x_4 = \mathbf{q} \bullet \mathbf{r} + t$, remains constant for all points of the selected section. On the other hand, the coordinate x_4 is generally different for different modulated positions of the same modulated atom. In our case (paarite and gladite), the three-dimensional structure is represented as the section $t = 0$, and therefore the coordinate x_4 is equal to $x_2/n = Y$, the coordinate in the n-fold supercell.

For the incommensurate case, all sections will yield a generally identical non-periodic structure, only with the origin shifted differently in each case. Moreover, in this case, every point of the modulation function has real meaning and is realized in the three-dimensional non-periodic structure. For commensurate cases, only a finite number of sections (*e.g.,* three sections for the three-fold structure) are realized and have real meaning (Fig. 3a).

In the subset $x_2 - x_4$ of superspace (Fig. 3b), the action of n can be shown as a pair of points (x_1, x_2, x_3, x_4) and ($x_1 + ½, x_2 + ½, x_3 + ½, x_4 + ½$). In Figure 3b, these points fall onto two out of the three (or, alternatively, five) occupied lattice-lines t of the $x_2 - x_4$ section of the four-dimensional lattice. This situation is valid for all odd-multiple superstructures, but not for even-multiple ones, typified in our study by salzburgite. In these, the second point falls half-way between the lattice levels t obtained in the $x_2 - x_4$ section; the relevant element of symmetry, however, does not operate outside the t sections realized. This is also the reason why it cannot be present as a symmetry element in the even-multiple supercell. From Figure 3b, it also is clear that the situation in the $x_2 - x_4$ section is independent of the choice of the first section t_0; it holds for all sets t_0, $t_0 + 1/3$, and $t_0 + 2/3$ (or the corresponding fourths or fifths).

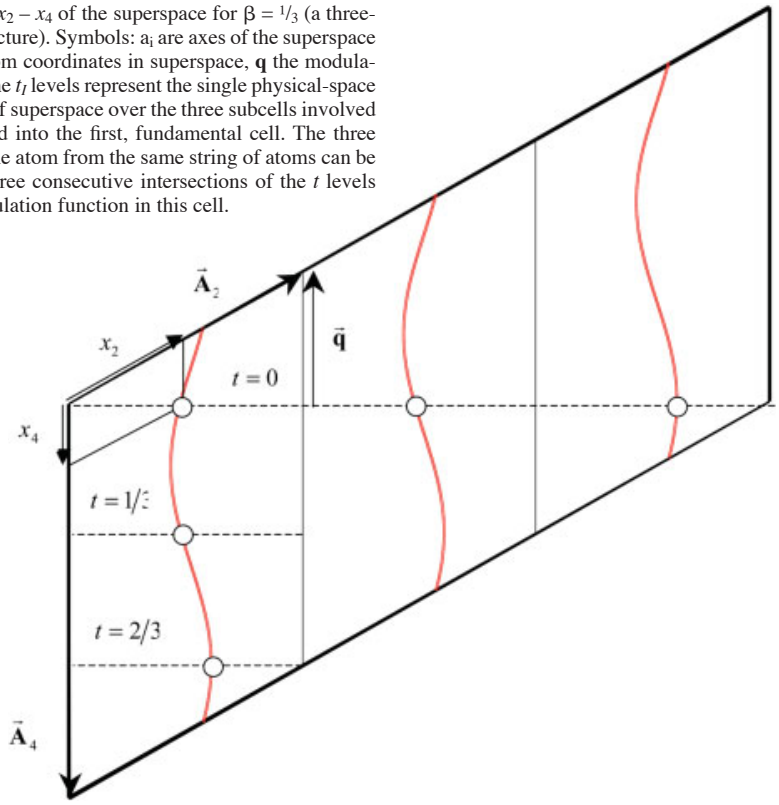

FIG. 3a. Subset $x_2 - x_4$ of the superspace for $\beta = 1/3$ (a three-fold superstructure). Symbols: a_i are axes of the superspace cell, x_i are atom coordinates in superspace, **q** the modulation vector. The t_I levels represent the single physical-space level cut out of superspace over the three subcells involved and condensed into the first, fundamental cell. The three positions of the atom from the same string of atoms can be seen as the three consecutive intersections of the t levels with the modulation function in this cell.

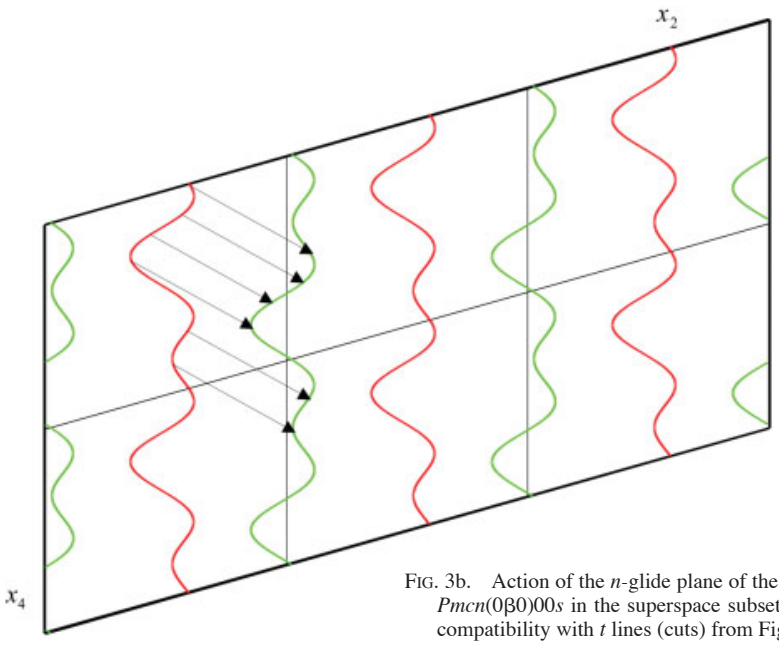

FIG. 3b. Action of the *n*-glide plane of the superspace group *Pmcn*(0β0)00*s* in the superspace subset $x_2 - x_4$. Note the compatibility with t lines (cuts) from Figure 3a.

However, not all symmetry elements of the supercell group are compatible with a free choice of the t_0 value. As a consequence, by selecting specific t_0 values, we can in general obtain different space-groups for the supercell. For example, the *c* glide plane from the superspace symbol yields equivalent points (x_1, x_2, x_3, x_4) and (x_1, $-x_2 + ½$, $x_3 + ½$, $-x_4 + ½$). For the odd-multiple superstructures ($\beta = 1/q$, q being an odd integer), the *c* glide plane is valid only for $t_0 = n/q$, or also for $t_0 = 1/(2q) + n/q$ (see Fig. 4a for the three-fold case, with the permissible t_0 values equal to 0, 1/6, 1/3, 3/6, 2/3, and 5/6). The *t* sections falling outside these values yield supercell groups without *c*. The same holds for the inversion center. Therefore, in the case of the odd-multiple superstructure, we can obtain either *Pmcn* or $Pm2_1n$, the latter one with a loss of both *c* and $\bar{1}$. For the even-multiple superstructures ($\beta = 1/q$), q being an even integer), the glide plane *n* is not acceptable, as shown above, and the glide plane *c* and the inversion center are no longer coexisting in the same t_0 sections. Thus the sections with general values of t_0 yield *Pm*,

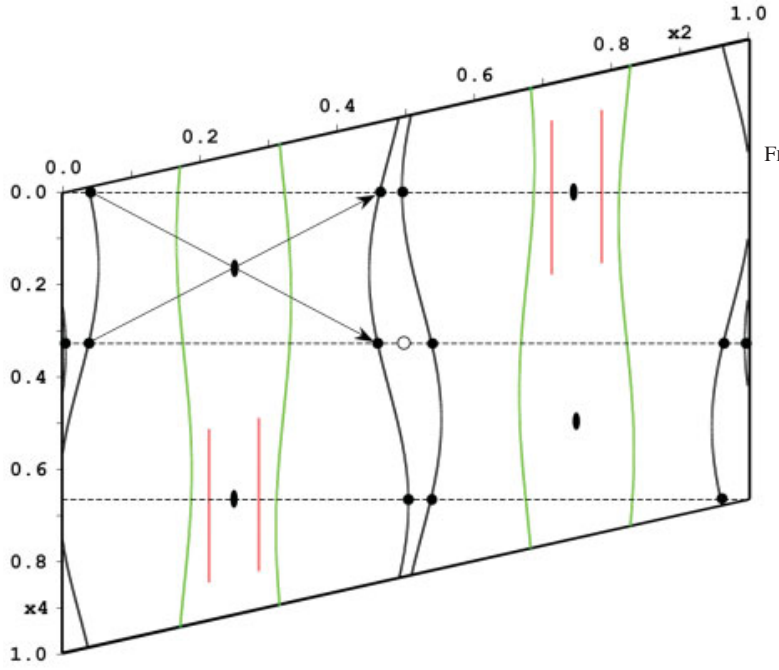

FIG. 4a. Action (x_1, $-x_2 + ½$, $x_3 + ½$, $x_4 + ½$) of the *c* glide plane of the superspace group *Pmcn*(0β0)00*s* in the $x_2 - x_4$ section of gladite (a three-fold superstructure) in which it "simulates" a symmetry centrum at (¼, ¼), *etc*. Atom "strings" describe the modulation of atom positions in the $x_2 - x_4$ section of superspace (compare with Fig. 10a).

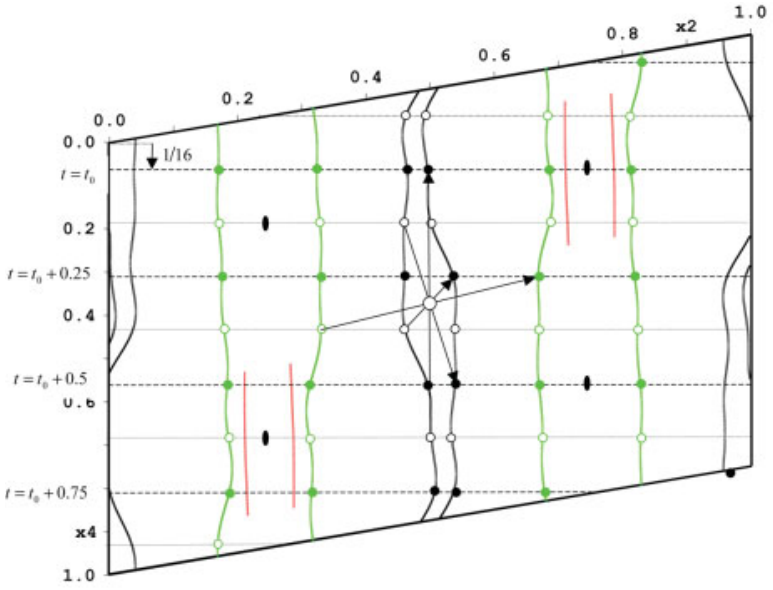

FIG. 4b. The centrosymmetric superspace group *Pmcn*(0β0)00*s* used for the description of the $Pmc2_1$ structure of salzburgite (a four-fold superstructure). Note a shift of t_0 by 1/16, the real $t_0 + n/4$ levels (dashed) and imaginary $t_0 + n/8$ levels (stippled), as well as the real (black) and imaginary (void) atoms on selected strings.

those with $t_0 = n/q$ and $t_0 = 1/(2q) + n/q$ give $P2_1/m$, whereas those at $t_0 = 1/(4q) + n/q$ and $t_0 = 3/(4q) + n/q$ give $Pmc2_1$, the space group observed in salzburgite, for which $t_0 = 1/16 + n/4$ or $3/16 + n/4$.

The full analysis of the superspace group *Pmcn* (0β0)00*s* for all possible rational modulation vectors $\beta = p/q$ leads to the supercell space-groups presented in Table 1.

Further application for odd-multiple superstructures is straightforward: atom parameters are obtained as points of intersection of *t* levels with the modulation function. It is not so for even-multiple superstructures. For the four-fold superstructure of *salzburgite*, t_0 had to be moved to 1/16 in order to preserve the *c*-glide planes, which in the $x_2 - x_4$ section "look" like centers of symmetry at (¼, ¼) (compare with the transformation matrix of the *c*-glide plane above) (Fig. 4b). In the case of the $Pmc2_1$ structure, we are sampling the centrosymmetric system of modulation functions of the superspace group *Pmcn*(0β0)00*s* by a *t* subset of levels with the initial t_0 value shifted against the origin of the superspace group. As a consequence, the atoms (points of intersection) on the $t_0 + n/4$ levels invert for $Pmc2_1$ (Fig. 4b) by the action of the original internal operator of the superspace group into atoms on the imaginary, $t_0 + 1/8$, 3/8,… levels. In order to describe these atom positions by a single modulation-function, analogous to that used for odd-multiple cases, we place a half of the atoms onto the 1/8, 3/8, *etc*. levels and bring them onto the 1/4 *etc*. levels by the action of the superspace center of inversion (and *vice versa* for the other half). This is done by increasing the number of waves used for each parameter to the mean value + seven harmonic functions (three pairs of trigonometric functions plus one sine function without its cosine counterpart). In this way, we keep the centrosymmetric superspace-group also for the case of an even-multiple superstructure.

Krupkaite has only a basic 11 Å cell with the space group $Pm2_1n$. Therefore, it cannot be described as a basic non-modulated structure with $b = 11.2$ Å, which has an inversion center. It follows from the table of all possible space-groups as presented in Table 1 that the modulation vector equals $\mathbf{q} = 2/1\mathbf{b}^* = 2\mathbf{b}^*$ ($p = 2$, $q = 1$) with $t_0 = ¼$ would fulfill the symmetry requirement.

TABLE 1. SUPERCELL SPACE-GROUPS DERIVED FROM THE SUPERSPACE GROUP *Pmcn* (0β0)00*s*

t_0	$q = 2n$ or $q = 2n + 1$, $p = 2m$	$q = 2n + 1$, $p = 2m + 1$
$0 + n/q$, $1/(2q) + n/q$ $\equiv n/(2q)$	$P2_1/m$	$Pmcn$
$1/(4q) + n/q$, $3/(4q) + n/q$ $\equiv (4n \pm 1)/(4q)$	$Pmc2_1$	$Pm2_1n$
general	Pm	$Pm2_1n$

This limiting case is similar to that for salzburgite, but it is more complicated. The situation is presented in Figure 5, where the refined modulation-curves of all cations are presented. The figure is similar to those for gladite, paarite and salzburgite, but here we had to draw three superspace cells to see all intersections through the selected hyperplane ($t_0 = ¼$). Let us concentrate on the two central modulation-curves (black and yellow in Fig. 5), which represent the modulation of the *M*2 (Pb,Bi) position. Both curves are related by an inversion center (the large open circles) in the four-dimensional superspace. The real atomic positions in the three-dimensional structure are the intersections of these curves with the hyperplane. It is clearly visible that these sites are not symmetrically related by an inversion center, the intersection with the yellow curve has a *y* coordinate close to ½, but the second one is considerably shifted from $y = ½$. This fully corresponds to the fact that the three-dimensional structure is non-centrosymmetric. The intersection of the yellow curve with the hyperplane is related through the inversion center in the superspace to a point on the black curve as indicated by the arrow. This point lies on the section $t_0 = ¾$, and the inversion operation results in two points of the independent modulation-curve being realized in the three-dimensional structure. This allowed us to use an average position and one harmonic wave to describe the structure as a modulated one. Figure 13 (see below) also shows that the main features of the unified description are the same for all compounds of the system, including the special case of krupkaite.

Determination of the Structure in Four Dimensions

The values of observed structure-factors were taken from the studies by Topa *et al*. (2000), Makovicky *et al*. (2001), and Balić-Žunić *et al*. (2002), where all the experimental details are to be found. Fundamental experimental values are quoted in Table 2. Starting parameters of the atoms were also obtained from these works. For each atom species (*i.e.*, an entire string of atoms, such as *M*1, *M*2, *S*1, etc., as defined above), these parameters were averaged over all the subcells of each individual structure to be refined. Refinements converged smoothly, and no problems in the refinements were observed. Copper atoms were left out in the initial cycle, and found later by inspection of the difference-Fourier maps in 3 + 1 dimensions. The behavior of Cu was described in the present study by crenel functions (Petříček *et al*. 1995), with the length (number of intersections of the crenel function on x_4 with the sampling *t* levels) adjusted during the study to fit the observed situation (these are the finite strings in Figs. 4a, b).

The positional parameters and anisotropic displacement parameters were refined by means of modulation functions. Full occupancy was assumed for all atoms refined. Only in the second part of the present study, for

the structures in which partial Cu occupancy of certain sites was observed (Topa *et al*. 2000, Balić-Žunić *et al*. 2002), the Cu occupancy of such sites was refined by an additional crenel function with a refinable occupancy-factor. The atoms Pb and Bi in the central, *M*2, sites of ribbons were not distinguished because of their very close atomic number; they were refined as Bi.

All refinements were started with the first harmonic only; it was also all what was needed for the description of the three-fold superstructure. For the five-fold superstructure, one more harmonic is required, whereas the situation for the four-fold superstructure has already been described. Refinement of modulated structures proceeds by refining the coefficients of a Fourier series, which, for the positional parameters, is

$$\mathbf{r}(x_4) = \mathbf{r}_{ave} + \sum_{n=1}^{\infty}\left[\mathbf{u}^x(n)\sin 2\pi n x_4 + \mathbf{u}^y(n)\cos 2\pi n x_4\right]$$

where n is the order of the harmonic. An example of the y-component displacement waves for Pb,Bi in the five-fold structure of paarite is shown in Figure 6. In the final step, we refined also the modulation waves of anisotropic displacement parameters of all atoms except copper to account for differences in coordination induced by the strong positional modulation. The resulting coefficients, and the equivalent isotropic displacement parameters as well as weighing functions and goodness-of-fit parameters, are indicated in Table 3. Anisotropic displacement parameters are in Table 4 (deposited). These being commensurate cases, structure factors were calculated using discrete t sections and not the entire modulation-waves, as is necessary for the incommensurate cases.

For all atoms situated on pure (*i.e.*, $\mathbf{t}_l = 0$) mirror planes, no superspace modulation exists in the $x_1 - x_4$ section. Modulation waves in the $x_2 - x_4$ and $x_3 - x_4$ sections show displacements $u_2(x_4)$ and $u_3(x_4)$, respectively, of *M*1 and *M*2 atoms [Bi and (Bi,Pb), in this order], copper and the three distinct S sites. Intercepts of the respective modulation-functions with the consecutive t levels are the only significant loci of these functions and represent consecutive atoms in the given string, subcell after subcell.

Results of the Refinements

Results of all refinements are the coefficients of an vorthogonalized harmonic function summarized in Table 3. The curve expressing the y coordinate of the *M*2 site in gladite, salzburgite and paarite as a function of x_4 is given in Figures 7a–c, superimposed on the Fourier map of the internal space $x_2 - x_4$. The essential unity of these displacements in the three superstructures becomes evident from these figures if the intersections of the y coordinate curves with the t levels are examined. Their full understanding requires comparison with the real structures (Figs. 8a–c) in which the respective

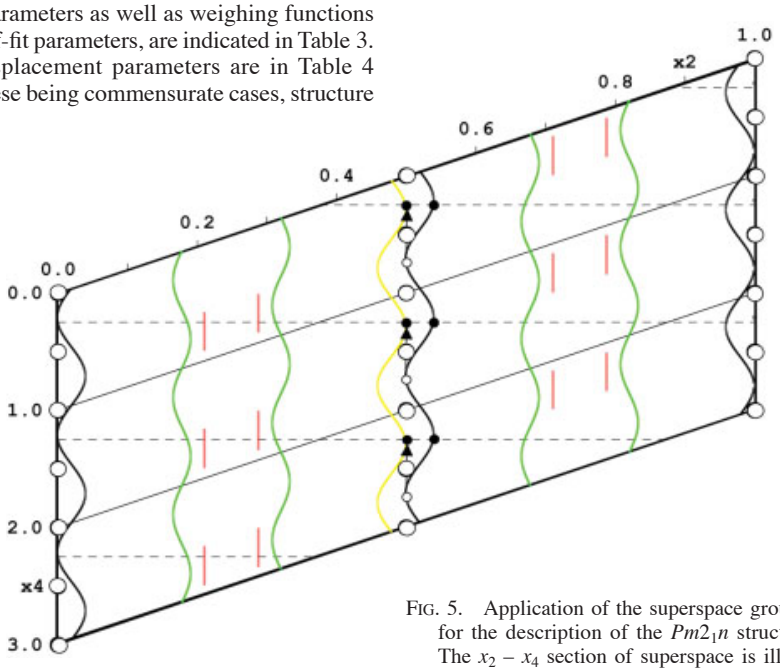

FIG. 5. Application of the superspace group *Pmcn*(0β0)00*s* for the description of the $Pm2_1n$ structure of krupkaite. The $x_2 - x_4$ section of superspace is illustrated, with the real t_0 = ¼ levels interleaved by imaginary t_0 = ¾ levels. Inversion centers of the superspace group are indicated by large void circles; real atoms are black, imaginary are void. Two central modulation curves, black and yellow, describe the modulation of *M*2 (Pb,Bi) position.

initial atoms and the strings of atoms generated from them by "modulation" are indicated.

The central *M*2 sites occupied by Pb have negative Δy and Δz values, those occupied by Bi have positive values. Whereas the Δy increments are nearly identical for all Pb and for all Bi positions, respectively, the Δz increment lacks this symmetry. The "first" Bi-occupied position after the Pb position(s) belongs to a bismuthinite-like ribbon and has a somewhat smaller Δz than those in the following krupkaite-like ribbons (Fig. 9).

The Δy increments of *M*1 atoms in gladite are smallest for the Bi positions adjacent, on the same ribbon side, to *M*2, but largest for the Bi1 atoms next to Cu-occupied tetrahedra. Those in the Bi_4S_6 ribbon have an intermediate Δy value. This is nearly true for paarite, although the scheme for the first-mentioned configuration is ambiguous (Fig. 9).

The *y* coordinate of Cu in the three structures is illustrated in Figures 10a–c on a background of the relevant positions of the Fourier map. The length of the non-zero part of the crenel function has been adjusted manually to cover all Cu positions in accordance with the structure. The alternative would have been sets of harmonic functions similar to those for *M*2.

TABLE 2. EXPERIMENTAL DETAILS

Crystal data	**Gladite**	**Oversubstituted gladite**	**Paarite**	**Salzburgite**	**Krupkaite**
Chemical formula	$Cu_{1.32}Pb_{1.37}Bi_{6.65}S_{12.30}$	$Cu_{1.55}Pb_{1.59}Bi_{6.43}S_{12.02}$	$Cu_{1.66}Pb_{1.71}Bi_{6.32}S_{11.99}$	$Cu_{1.60}Pb_{1.62}Bi_{6.38}S_{11.97}$	$Cu_{2.00}Pb_{2.03}Bi_{5.99}S_{12.04}$
Cell setting	Orthorhombic	Orthorhombic	Orthorhombic	Orthorhombic	Orthorhombic
Superspace group	*Pmcn*(0β0)00*s*	*Pmcn*(0β0)00*s*	*Pmcn*(0β0)00*s*	*Pmcn*(0β0)00*s*	*Pmcn*(0β0)00*s*
a (Å)	4.0044	4.0100	4.007	4.0074	4.0145
b (Å)	11.1918	11.1963	11.1996	11.2031	11.2023
c (Å)	11.4795	11.502	11.5123	11.5133	11.5604
V (Å^3)	514.5	516.4	516.6	516.9	519.9
Formula units	4	4	4	4	4
Modulation wavevector	**q** = 1/3 **b***	**q** = 1/3 **b***	**q** = 1/5 **b***	**q** = 1/4 **b***	**q** = 2 **b***
Data collection					
Diffractometer	Bruker AXS 4-circle	Bruker AXS 4-circle	Bruker AXS 4-circle	Bruker AXS 4-circle	Bruker AXS 4-circle
Radiation type	Mo*K*α	Mo*K*α	Mo*K*α	Mo*K*α	Mo*K*α
Wavelength (Å)	0.71073	0.71073	0.71073	0.71073	0.71073
Absorption correction type	equiv. reflections	equiv. reflections	equiv. reflections	equiv. reflections	equiv. reflections
Absorption coeff. μ (mm^{-1})	70.198	70.089	70.126	69.98	69.89
T_{min}/T_{max}	0.001/0.013	0.003/0.019	0.001/0.013	0.008/0.032	0.003/0.021
Range of *h*,*k*,*l*,*m*	$-4 \rightarrow h \rightarrow 3$	$-4 \rightarrow h \rightarrow 5$	$-5 \rightarrow h \rightarrow 4$	$-4 \rightarrow h \rightarrow 5$	$-4 \rightarrow h \rightarrow 5$
	$-14 \rightarrow k \rightarrow 14$	$-14 \rightarrow k \rightarrow 14$	$-14 \rightarrow k \rightarrow 14$	$-14 \rightarrow k \rightarrow 13$	$-14 \rightarrow k \rightarrow 14$
	$-13 \rightarrow l \rightarrow 14$	$-14 \rightarrow l \rightarrow 13$	$-14 \rightarrow l \rightarrow 14$	$-13 \rightarrow l \rightarrow 13$	$-14 \rightarrow l \rightarrow 13$
	$-1 \rightarrow m \rightarrow 1$	$-1 \rightarrow m \rightarrow 1$	$-2 \rightarrow m \rightarrow 2$	$-2 \rightarrow m \rightarrow 2$	
No. of measured reflections	8856	8954	15242	12470	2972
No. of unique reflections	1745	1800	3050	3717	1145
No. of observed reflections	1355	1472	1755	2434	1082
No. of main reflections	583	600	524	815	1145
No. of satellite reflections	1163	1200	848 + 383	1242 + 374	-
Criterion for observed reflections	$I > 3\sigma(I)$	$I > 3\sigma(I)$	$I > 3\sigma(I)$	$I > 3\sigma(I)$	$I > 3\sigma(I)$
R_{int}	0.0590	0.0543	0.0901	0.0734	0.0651
Refinement					
Refinement on	F^2	F^2	F^2	F^2	F^2
R, *wR* (all reflections)	0.0547 / 0.1021	0.0450 / 0.0813	0.1006 / 0.1308	0.0706 / 0.1166	0.0384 / 0.0880
R, *wR* (main reflections)	0.0462 / 0.0973	0.0388 / 0.0813	0.0599 / 0.1170	0.0411 / 0.0830	-
R, *wR* (1st order satellites)	0.0656 / 0.1089	0.0531 / 0.0814	0.0853 / 0.1228	0.0829 / 0.1484	-
R, *wR* (2nd order satellites)	-	-	0.2745 / 0.2881	0.1912 / 0.2828	-
S	2.32	2.06	2.10	1.87	2.27
No. of parameters	97	101	159	250	101
Weighting scheme	$w = [\sigma^2(I)+(0.01I)^2]^{-1}$	$w = [\sigma^2(I)+(0.01I)^2]^{-1}$	$w = [\sigma^2(I)+(0.01I)^2]^{-1}$	$w = [\sigma^2(I)+(0.01I)^2]^{-1}$	$w = [\sigma^2(I)+(0.01I)^2]^{-1}$
$(\Delta / s.u.)_{max}$	0.0079	0.0222	0.0071	0.0363	0.0432
Extinction correction	None	None	None	None	None

The source of atomic scattering factors is the International Tables for X-ray Crystallography (1992, Volume C).

TABLE 3. FINAL VALUES OF COORDINATES AND FOURIER AMPLITUDES OF DISPLACIVE MODULATION FUNCTIONS

Atom	Δ	occ	x_4^0	Wave	x	y	z	U_{eq}/U_{iso} (Å^2)
Gladite								
*M*1					0.25	0.17747(6)	0.51813(6)	0.0432(2)
				s,1	0	-0.00947(8)	-0.00937(8)	
				c,1	0	-0.00574(7)	0.00686(8)	
*M*2					0.25	0.52394(6)	0.33747(6)	0.0466(2)
				s,1	0	-0.02493(8)	-0.01937(8)	
				c,1	0	-0.01421(8)	-0.00472(8)	
Cu1	1/3		0.25		0.25	0.7137(3)	0.7206(3)	0.0499(11)
S1					0.25	-0.0563(3)	0.3784(3)	0.0413(11)
				s,1	0	-0.0038(4)	-0.0112(4)	
				c,1	0	0.0026(4)	-0.0075(5)	
S2					0.25	0.6310(4)	0.5471(3)	0.0410(11)
				s,1	0	-0.0086(4)	-0.0087(5)	
				c,1	0	0.0079(4)	-0.0024(4)	
S3					0.25	0.3049(3)	0.7159(3)	0.0391(10)
				s,1	0	-0.0029(4)	-0.0092(4)	
Oversubstituted gladite								
*M*1		1.0			0.25	0.17793(4)	0.51838(4)	0.03650(15)
				s,1	0	-0.00748(6)	-0.00922(5)	
				c,1	0	-0.00521(5)	0.00575(5)	
*M*2		1.0			0.25	0.52284(5)	0.33716(4)	0.04163(16)
				s,1	0	-0.02301(6)	-0.02089(6)	
				c,1	0	-0.01507(6)	-0.00378(6)	
Cu1	1/3	1.0	0.25		0.25	0.7141(2)	0.7206(2)	0.0426(7)
Cu2	1/3	0.136(10)	0.5		0.25	0.7057(15)	0.7324(15)	0.040(7)
S1		1			0.25	-0.0563(2)	0.3782(2)	0.0330(7)
				s,1	0	-0.0038(3)	-0.0111(3)	
				c,1	0	0.0020(3)	-0.0061(3)	
S2		1			0.25	0.6317(3)	0.5473(2)	0.0344(8)
				s,1	0	-0.0092(3)	-0.0082(3)	
				c,1	0	0.0063(3)	-0.0021(3)	
S3		1			0.25	0.3052(2)	0.7158(2)	0.0324(7)
				s,1	0	-0.0026(3)	-0.0089(3)	
				c,1	0	0.0047(3)	0.0030(3)	
Paarite								
*M*1					0.25	0.17807(6)	0.51824(6)	0.0435(2)
				s,1	0	-0.00949(8)	-0.01146(9)	
				c,1	0	-0.00361(7)	0.00488(10)	
				s,2	0	-0.00250(10)	0.00195(14)	
				c,2	0	-0.00315(10)	-0.00049(14)	
*M*2					0.25	0.52211(6)	0.33656(7)	0.0480(2)
				s,1	0	-0.02491(8)	-0.02263(10)	
				c,1	0	-0.01018(8)	-0.00270(11)	
				s,2	0	-0.00721(9)	-0.00449(13)	
				c,2	0	0.00689(10)	0.00308(15)	
Cu1	1/3		1.0		0.25	0.7123(3)	0.7196(3)	0.0518(11)
				o,1	0	-0.0023(3)	0.0001(4)	
S1					0.25	-0.0558(3)	0.3786(4)	0.0411(11)
				s,1	0	-0.0043(4)	-0.0128(5)	
				c,1	0	0.0020(4)	-0.0048(6)	
				s,2	0	0.0005(6)	0.0017(8)	
				c,2	0	0.0014(6)	-0.0012(8)	
S2					0.25	0.6317(3)	0.5468(4)	0.0415(12)
				s,1	0	-0.0091(4)	-0.0110(5)	
				c,1	0	0.0056(5)	-0.0016(5)	
				s,2	0	-0.0041(6)	-0.0009(8)	
				c,2	0	-0.0017(6)	0.0019(8)	
S3					0.25	0.3045(3)	0.7158(4)	0.0400(11)
				s,1	0	-0.0022(4)	-0.0116(5)	
				c,1	0	0.0047(4)	0.0031(6)	
				s,2	0	-0.0003(6)	-0.0003(8)	
				c,2	0	-0.0015(6)	-0.0027(8)	
Salzburgite								
*M*1					0.25	0.17810(5)	0.51825(5)	0.02951(19)
				s,1	0	-0.00802(7)	-0.00918(7)	
				c,1	0	-0.00397(7)	0.00451(7)	
				s,2	0	-0.00147(12)	0.00160(13)	
				c,2	0	-0.00249(11)	-0.00069(13)	
				s,3	0	0.00042(19)	0.0001(2)	
				c,3	0	-0.00213(19)	-0.0011(2)	
				s,4	0	0.0029(3)	0	
*M*2					0.25	0.52239(6)	0.33675(6)	0.0356(2)
				s,1	0	-0.02227(8)	-0.01901(8)	
				c,1	0	-0.01120(10)	-0.00256(10)	
				s,2	0	-0.00717(12)	-0.00433(13)	
				c,2	0	0.00615(12)	0.00229(15)	
				s,3	0	-0.00346(16)	-0.0012(2)	
				c,3	0	-0.00179(19)	-0.0003(2)	
				s,4	0	-0.00517(14)	-0.00412(19)	
Cu1	1/3		1.0		0.25	0.7131(3)	0.7195(3)	0.0389(10)
				o,1	0	-0.0017(4)	0.0001(4)	
				o,2	0	0.0006(7)	-0.0009(10)	
S1					0.25	-0.0566(3)	0.3784(3)	0.0276(11)
				s,1	0	-0.0039(4)	-0.0109(4)	
				c,1	0	0.0016(4)	-0.0058(5)	
				s,2	0	0.0000(7)	0.0015(9)	
				c,2	0	-0.0001(7)	-0.0005(8)	
				s,3	0	0.0002(13)	0.0012(16)	
				c,3	0	0.0015(12)	-0.0003(15)	
				s,4	0	0.0006(8)	0.0000(12)	
S2					0.25	0.6317(3)	0.5466(3)	0.0255(11)
				s,1	0	-0.0082(5)	-0.0096(5)	
				c,1	0	0.0054(5)	-0.0013(5)	
				s,2	0	-0.0034(7)	-0.0012(7)	
				c,2	0	-0.0007(7)	0.0015(8)	
				s,3	0	-0.0003(12)	-0.0042(14)	
				c,3	0	0.0040(12)	0.0010(16)	
				s,4	0	-0.0050(10)	0.0002(14)	
S3					0.25	0.3047(3)	0.7151(4)	0.0257(12)
				s,1	0	-0.0017(4)	-0.0076(5)	
				c,1	0	0.0047(4)	0.0038(5)	
				s,2	0	0.0027(7)	-0.0002(9)	
				c,2	0	-0.0001(7)	-0.0014(7)	
				s,3	0	-0.0003(12)	-0.0004(14)	
				c,3	0	-0.0016(12)	-0.0022(16)	
				s,4	0	-0.002(2)	0.010(3)	
Krupkaite								
*M*1					0.25	0.17885(8)	0.51850(8)	0.0331(3)
				s,1	0	-0.01258(14)	0	
*M*2					0.25	0.52013(9)	0.33561(9)	0.0370(3)
				s,1	0	0.02023(9)	0.00961(13)	
Cu1	1/3		1.0		0.25	0.7114(4)	0.7295(4)	0.0405(14)
S1					0.25	-0.0561(5)	0.3787(5)	0.0306(15)
				s,1	0	0.0052(8)	-0.0004(8)	
S2					0.25	0.6324(5)	0.5465(4)	0.0306(15)
				s,1	0	-0.086(6)	0.003(7)	
S3					0.25	0.3047(5)	0.7160(4)	0.0317(15)
				s,1	0	-0.0004(9)	-0.0017(9)	

The waves are sorted by the term (**s** for sine, **c** for cosine, **o** for orthogonalized functions) and the order of the harmonic **n**. Crenel function coefficients, x_4^0 and Δ, express the center and the length, respectively, of the interval in which the copper atom is present.

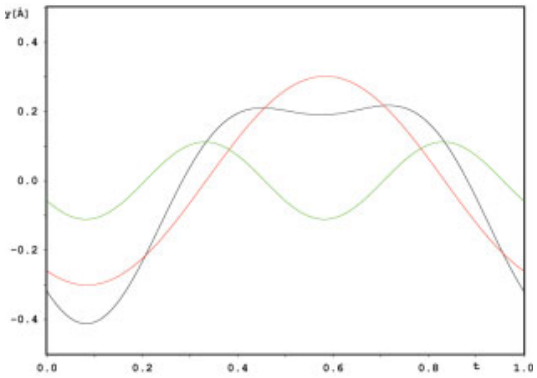

FIG. 6. Two component waves and the final Δy displacement wave (black) for *M*2 (Pb, Bi) in the five-fold structure of paarite. Only the points on levels $t = 0 + n/5$ express real displacements of atoms.

The full meaning of these data emerges from Figures 11–12, in which displacements Δy and Δz of all atoms in the fundamental 11 Å cell can be traced. Again, their interpretation is intimately connected with Figures 8a–c of the full structure. For the sake of understanding these figures, it has to be stressed again that, in the sections $x_2 - x_4$ and $x_3 - x_4$, the x_2 (x_3) axis represents the y (z) coordinate in the fundamental 11 Å cell, whereas x_4 indicates the full modulation-period (which is equal to three fundamental-cell lengths for gladite). Atoms lie on the intersection of their modulation curves [$y_{ave} + \Delta y$] and [$z_{ave} + \Delta z$], respectively, with the t levels, which in upward succession indicate the successive "subcells" of the modulated structure. For the $x_2 - x_4$ section, these

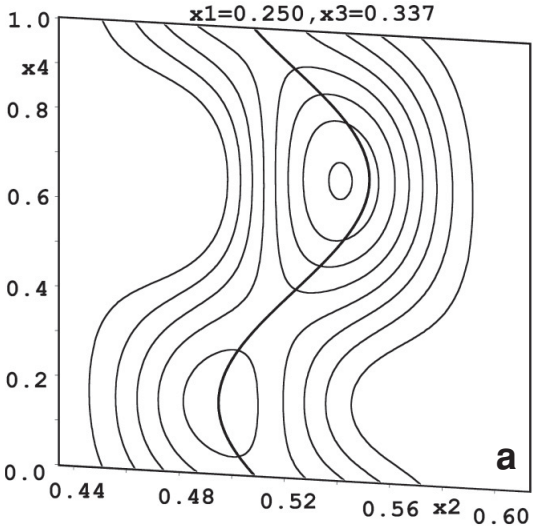

FIG. 7a–c. The y coordinate curves for "Pb" (*i.e.*, *M*2) atom string in the crystal structures of gladite, salzburgite and paarite, plotted on the background of Fourier maps of the internal space $x_2 - x_4$.

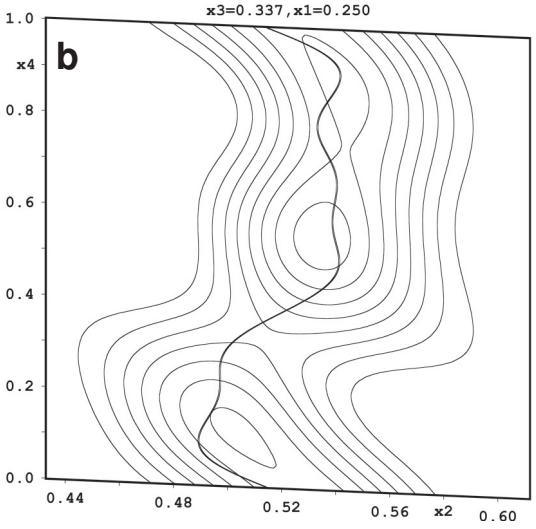

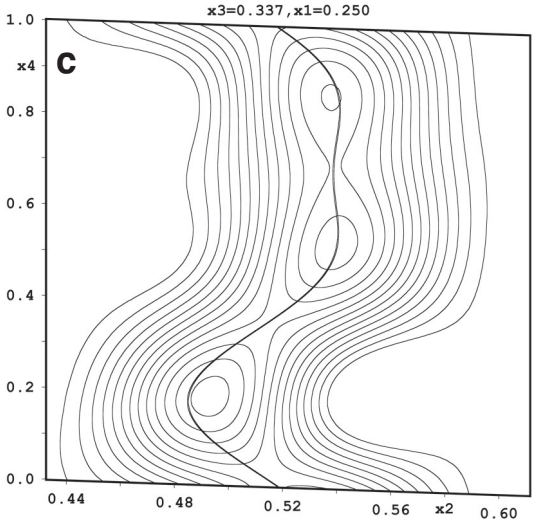

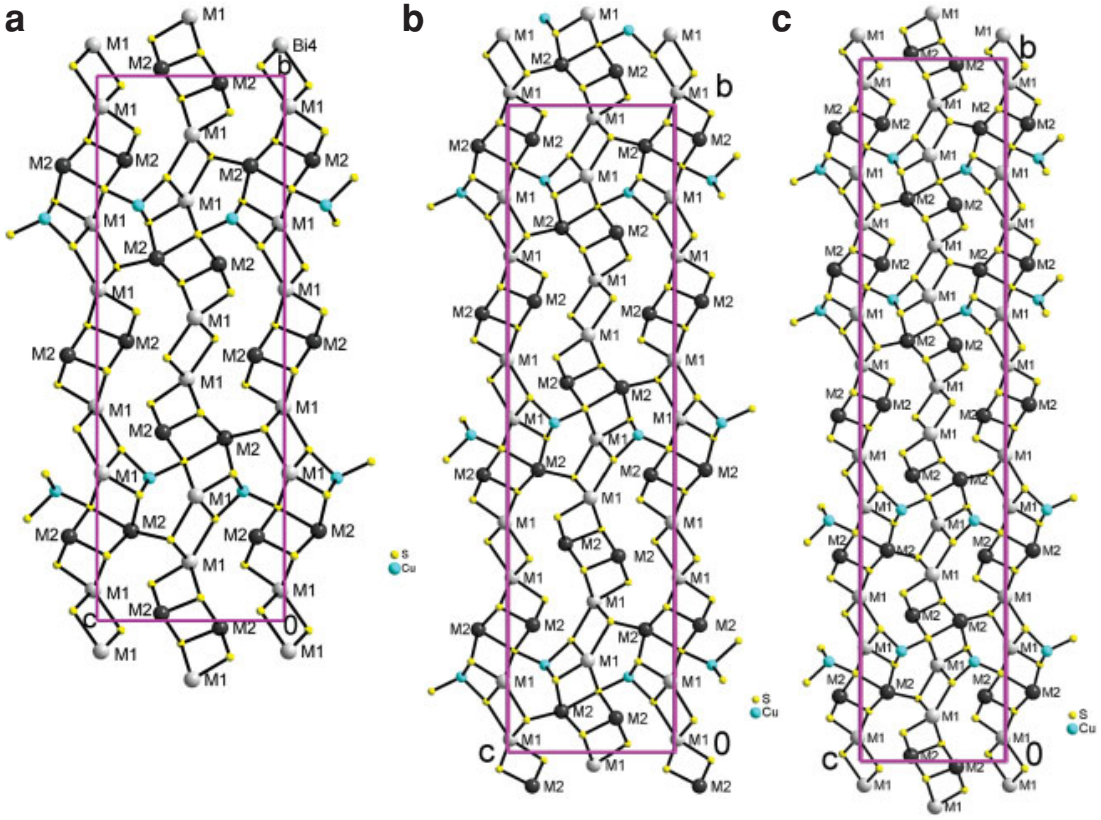

FIG. 8. The crystal structures of (a) gladite, (b) salzburgite and (c) paarite, with the cation strings parallel to *b* indicated by labeling. Atoms of sulfur are shown in yellow, and atoms of copper, in green.

t levels are obvious; however, for the $x_3 - x_4$ section, they move ("sweep the field") upward as the value of x_4 increases. To use the example of gladite, the first *t* level moves with the increasing x_4 value from 0.0 to 0.33, the second *t* level follows the x_4 value from 0.33 to 0.66, and the third one from 0.66 to 1.00. Thus we must estimate the x_2 coordinate of the atom first (*e.g.*, by reading it off Fig. 11) in order to evaluate its x_3 (or Δz) coordinate. Let us not forget the starting phase-shift $t_0 = 1/16$ for salzburgite.

Figures 11a and 12a for *gladite* are easiest to interpret. The (Pb,Bi) *M*2 curves in Figure 11a show Δy values for the Bi_4S_6 ribbon (at $t = 1/3$) to be larger than those for the $Cu_2Pb_2Bi_2S_6$ ribbon. This is a result of larger lateral asymmetry in the bond scheme of $Bi(2)S_5$ pyramids in comparison with the Pb(2) pyramids. The same explanation holds for the movements of S2. The Bi1 curves around the 1/3 and 2/3 levels show a larger Δy difference for Cu-free ribbon contacts than for the Cu-populated ones. The two Bi1 atoms illustrated belong to two distinct intermeshed ribbons, and the latter trend indicates a deeper insertion of these ribbons into each other's interspaces.

The $x_3 - x_4$ plot reveals a sinusoidal movement of the *z* coordinate for all large cations. Modulations of the (Pb,Bi)2 positions are parallel for all four (Pb,Bi)2 strings in the supercell (Fig. 12a); that for Bi1 shows a decrease in the difference of *z* coordinates for pure Bi_4S_6 ribbons. The Bi1 curves that are adjacent in the $x_3 - x_4$ plot belong to Bi1 atoms at the opposite ends of the same ribbon. Thus, their Δz gap can be taken as a measure of ribbon rotation about its central 2_1 axis. The Bi_4S_6 ribbons in gladite are therefore closer to parallelism with the [010] direction, whereas the $Cu_2Pb_2Bi_2S_6$ ribbons are more rotated, toward the Cu atoms attached to them (Fig. 8a).

Owing to the smaller degree of rotation of the Bi_4S_6 ribbons and a more pronounced rotation of two consecutive $Cu_2Pb_2Bi_2S_6$ ribbons that are hinged onto the former ones *via* Cu-free contacts (Fig. 8a) and mutually *via* Cu-containing contacts, sinusoidal shifts of (especially) the central (Pb,Bi)2 atoms, $-\Delta z$ for the

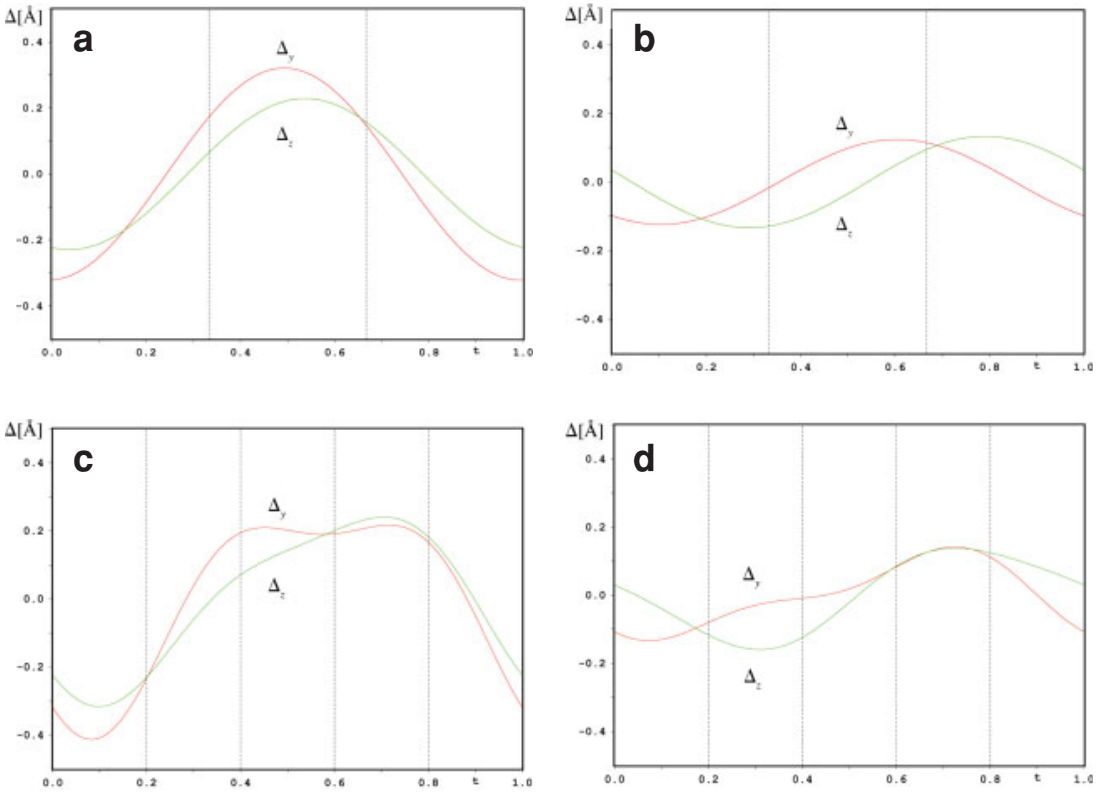

FIG. 9. Curves of Δy and Δz for $M2$ (Pb, Bi) and $M1$ (Bi) positions in (a, b) gladite and (c, d) paarite. Green curve: Δz, red curve: Δy. The interpretation of t levels for Δy and Δz, respectively, is explained in the text.

first subcell (t = 1/3), and $+\Delta z$ for the third subcell (t = 2/3), are generated. This kind of information can also be derived from discretely refined structures, but it requires a more laborious analysis.

The plots $x_2 - x_4$ and $x_3 - x_4$ of *salzburgite* (a four-fold superstructure) show the same features (Figs. 11b and 12b). Their "stiff" appearance is connected with the presence of a single Bi_4S_6 ribbon in any one [010] sequence of four ribbons; this ribbon shows lesser rotation. The "stiff" Δy curves for Bi1 again are more distant from each other in Cu-free intervals, and closer in the intervening Cu-containing intervals.

Paarite (Figs. 11c, 12c) contains only one Bi_4S_6 ribbon in a [010] string of five distinct ribbons. It has a pair of Cu-containing ribbon contacts interspersed between three Cu-free contacts. Thus, Δy of the (Pb,Bi)2 curve lies between those of salzburgite and gladite, whereas the Bi1 curve is straight for x_4 from 0.0 to 0.4, and for its symmetry-equivalent, and shows constriction of the Bi1 – Bi1 curve interspace in the Cu-containing parts; the same explanation as for salzburgite applies. The $x_3 - x_4$ diagram shows sinusoidal trends that are nearly identical with those in gladite; an additional $-\Delta z$ shift of Pb is observed in the first subcell, indicating its position in the trigonal prismatic site of the inter-ribbon space. The interspace of Bi1–Bi1 curves again expresses lesser rotation of the Bi_4S_6 ribbon in respect to the krupkaite-like ribbons.

The $x_2 - x_4$ diagram of *oversubstituted gladite* is virtually identical with that for stoichiometric gladite. The refined, partly occupied, position of Cu2 is shifted slightly in the y coordinate against the fully occupied Cu1 positions (Fig. 13). Positional shifts for other cations, connected with the vacancy of the Cu2 positions in the previous structures, are slightly smaller in this case, owing to only partial vacancies at Cu2 sites.

Table 5 shows the fractional coordinates of atoms derived from the superspace refinement of the gladite structure, compared to those refined as discrete atoms in the 33 Å supercell under the same conditions of refinement. These coordinates are almost identical, which reflects the fact that both descriptions are equivalent where the highest possible number of modulation waves is used. Table 6 shows the selected interatomic

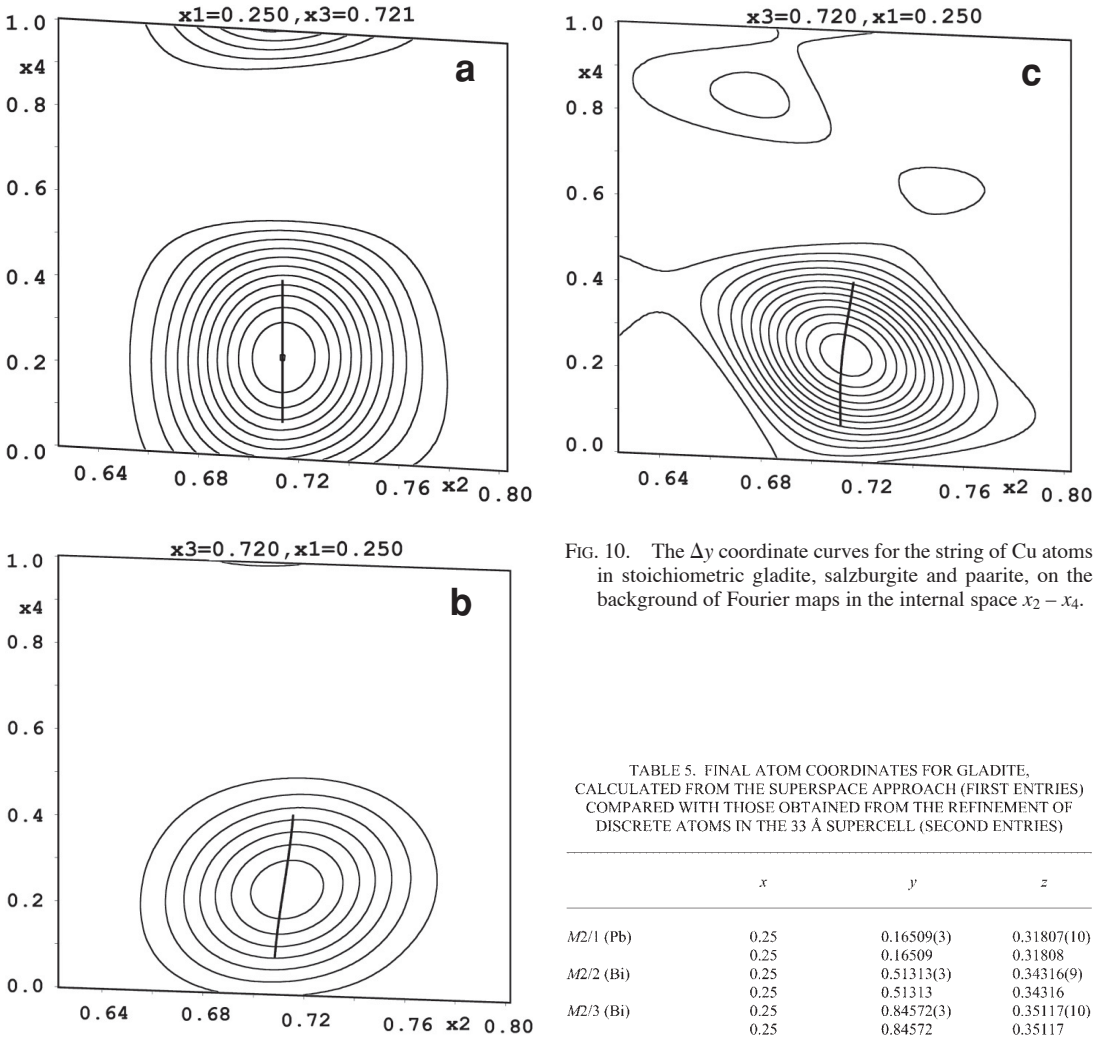

FIG. 10. The Δy coordinate curves for the string of Cu atoms in stoichiometric gladite, salzburgite and paarite, on the background of Fourier maps in the internal space $x_2 - x_4$.

cation–anion distances in gladite, obtained by the modulated structure approach.

EPILOGUE

Our results show the great versatility and universality of the superspace approach developed for modulated structures. Properly applied, it is capable of describing not only modulations over several basic cells, but also the modulations with several modulation-waves inside one basic cell. It should be stressed, however, that amenability of a family of related structures to the superspace refinement as commensurately modulated structures does not automatically turn them into typical modulated structures. In the commensurately modulated description, we fit continuous sinusoidal functions to a

TABLE 5. FINAL ATOM COORDINATES FOR GLADITE, CALCULATED FROM THE SUPERSPACE APPROACH (FIRST ENTRIES) COMPARED WITH THOSE OBTAINED FROM THE REFINEMENT OF DISCRETE ATOMS IN THE 33 Å SUPERCELL (SECOND ENTRIES)

	x	*y*	*z*
*M*2/1 (Pb)	0.25	0.16509(3)	0.31807(10)
	0.25	0.16509	0.31808
*M*2/2 (Bi)	0.25	0.51313(3)	0.34316(9)
	0.25	0.51313	0.34316
*M*2/3 (Bi)	0.25	0.84572(3)	0.35117(10)
	0.25	0.84572	0.35117
*M*1/1 (Bi)	0.25	0.05623(3)	0.52112(9)
	0.25	0.05623	0.52112
*M*1/2 (Bi)	0.25	0.39201(3)	0.50692(9)
	0.25	0.39201	0.50692(9)
*M*1/3 (Bi)	0.25	0.72923(3)	0.52636(9)
	0.25	0.72923	0.52636
S1/1	0.25	-0.01777(19)	0.3723(6)
	0.25	-0.01777	0.3723
S1/2	0.25	0.31306(18)	0.3710(6)
	0.25	0.31306	0.3710
S1/3	0.25	0.64840(19)	0.3919(6)
	0.25	0.64840	0.3919
S2/1	0.25	0.20821(20)	0.5380(6)
	0.25	0.20821	0.5380
S2/2	0.25	0.54190(18)	0.5518(5)
	0.25	0.54189	0.5518
S2/3	0.25	0.88090(18)	0.5515(6)
	0.25	0.88089	0.5515
S3/1	0.25	0.10229(18)	0.7134(6)
	0.25	0.10229	0.7134
S3/2	0.25	0.43318(17)	0.7088(6)
	0.25	0.43318	0.7088
S3/3	0.25	0.76942(19)	0.7255(5)
	0.25	0.76942	0.7255
Cu1/1	0.25	0.23789(11)	0.7206(3)
	0.25	0.23789	0.7206

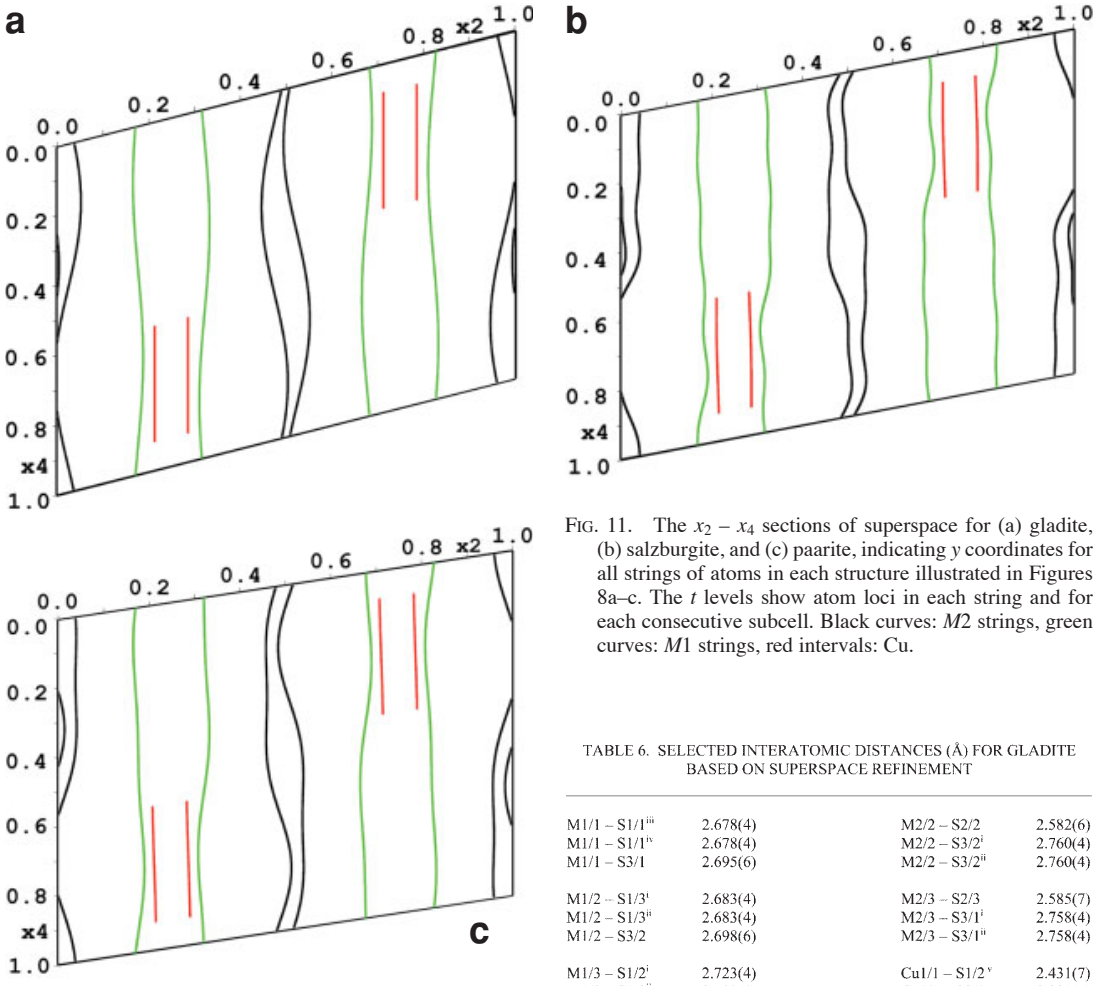

FIG. 11. The $x_2 - x_4$ sections of superspace for (a) gladite, (b) salzburgite, and (c) paarite, indicating y coordinates for all strings of atoms in each structure illustrated in Figures 8a–c. The t levels show atom loci in each string and for each consecutive subcell. Black curves: $M2$ strings, green curves: $M1$ strings, red intervals: Cu.

TABLE 6. SELECTED INTERATOMIC DISTANCES (Å) FOR GLADITE BASED ON SUPERSPACE REFINEMENT

M1/1 – S1/1^{iii}	2.678(4)	M2/2 – S2/2	2.582(6)
M1/1 – S1/1^{iv}	2.678(4)	M2/2 – S3/2^{i}	2.760(4)
M1/1 – S3/1	2.695(6)	M2/2 – S3/2^{ii}	2.760(4)
M1/2 – S1/3^{i}	2.683(4)	M2/3 – S2/3	2.585(7)
M1/2 – S1/3^{ii}	2.683(4)	M2/3 – S3/1^{i}	2.758(4)
M1/2 – S3/2	2.698(6)	M2/3 – S3/1^{ii}	2.758(4)
M1/3 – S1/2^{i}	2.723(4)	Cu1/1 – S1/2^{v}	2.431(7)
M1/3 – S1/2^{ii}	2.723(4)	Cu1/1 – S2/1	2.321(7)
M1/3 – S3/3	2.654(6)	Cu1/1 – S3/3^{vi}	2.348(4)
		Cu1/1 – S3/3^{vii}	2.348(4)
M2/1 – S2/1	2.911(7)		
M2/1 – S2/3^{i}	2.938(5)		
M2/1 – S2/3^{ii}	2.938(5)		

Symmetry codes: (i) $-x, 1-y, 1-z$, (ii) $1-x, 1-y, 1-z$, (iii) $-x, -y, 1-z$, (iv) $1-x, -y, 1-z$, (v) $-x, 1/2+y, 1/2-z$, (vi) $-x, -1/2+y, 3/2-z$, (vii) $1-x, -1/2+y, 3/2-z$.

set of discrete values at discrete, periodically repeating sites. A modulated nature of the structure is obvious in the situations where we deal with "lock-in" members of a series of incommensurately modulated structures. It is not the case where such a reference frame is missing, as in the present instance.

The structures treated in this paper can be, and also were, refined using discrete atoms and three-dimensional space-groups instead of modulated strings of atoms and a superspace group. Structural descriptions of this family were given in terms of two coexisting types of M_4S_6 ribbons arranged into ordered patterns (Ohmasa & Nowacki 1970a) as well as in modular terms, referring to the planes of tetrahedra fully occupied by Cu atoms and to the width of the copper-free intervals (moduli) between them (Topa *et al.* 2000, Makovicky *et al.* 2001, Ferraris *et al.* 2004). The present description, as commensurately modulated structures, besides giving an alternative method of structure refinement, adds one more approach to these structure descriptions, revealing especially the global adjustments of the structure framework. The atom-coordinate curves are not as easy to interpret as the interatomic distances but, properly analyzed, they reflect the overall positional (or displacement, occupancy) trends, which remain usually submerged in localized descriptions.

The structures of the aikinite–bismuthinite series are not typical modulated structures, such as those of

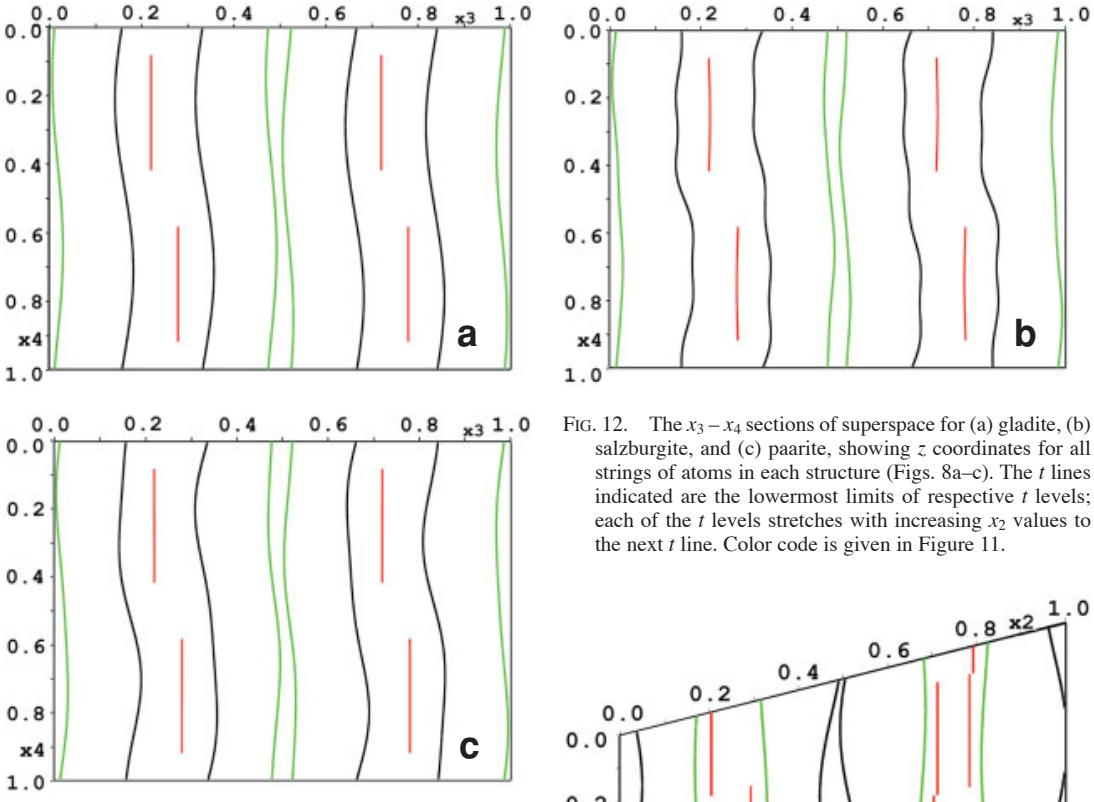

FIG. 12. The $x_3 - x_4$ sections of superspace for (a) gladite, (b) salzburgite, and (c) paarite, showing z coordinates for all strings of atoms in each structure (Figs. 8a–c). The t lines indicated are the lowermost limits of respective t levels; each of the t levels stretches with increasing x_2 values to the next t line. Color code is given in Figure 11.

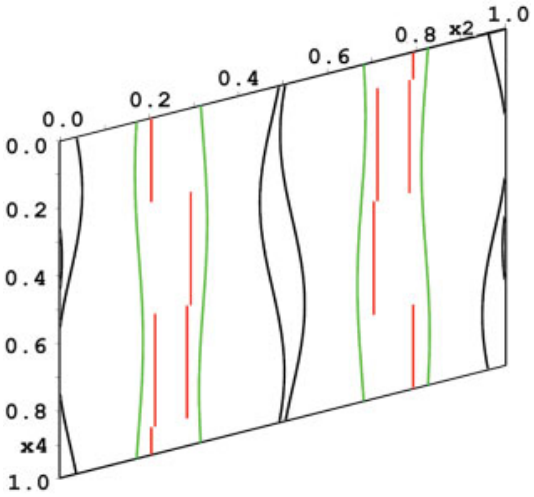

FIG. 13. The $x_2 - x_4$ section of superspace for oversubstituted gladite. The "paired" and "unpaired" crenel function intervals describe y coordinates of a fully occupied Cu1 and partly occupied Cu2 position, respectively.

Na_2CO_3 (deJong & Tuinstra 1979, Hogervorst *et al.* 1979, Zubkova *et al.* 2002, Dušek *et al.* 2003), for example. At best, they can be classified as *interface-modulated structures* (Amelinckx 1979), where the interfaces modulating the basic structure are the (010) planes with tetrahedra occupied by Cu, and the Pb sites adjacent to these. It means that these structures are a boundary case, eminently suitable also for the aforementioned alternative, modular approach. Still, owing to the introduction of the crenel function, the present series was successfully treated as a modulated structure by a superspace approach.

ACKNOWLEDGEMENTS

This project was partly funded by the Danish Research Council for Natural Sciences.

REFERENCES

AMELINCKX, S. (1979): Survey of modulated structure phenomena. *In* Modulated Structures – 1979 (J.M. Cowley, J.B. Cohen, M.B. Salamon & B.J. Wuensch, eds.). *Am. Inst. Phys., Conf. Proc.* **53**, 102-113.

BALIĆ-ŽUNIĆ, T., TOPA, D. & MAKOVICKY, E. (2002): The crystal structure of emilite, $Cu_{10.7}Pb_{10.7}Bi_{21.3}S_{48}$, the second 45 Å derivative of the bismuthinite–aikinite solid-solution series. *Can. Mineral.* **40**, 239-245.

CHEN, T.T., KIRCHNER, E. & PAAR, W. (1978): Friedrichite, $Cu_5Pb_5Bi_7S_{18}$, a new member of the aikinite–bismuthinite series. *Can. Mineral.* **16**, 127-130.

DEJONG, F. & TUINSTRA, F. (1979): Structural changes at the incommensurate phase transition of Na_2CO_3. *In* Modulated Structures – 1979 (J.M. Cowley, J.B. Cohen, M.B.

Salamon & B.J. Wuensch, eds.). *Am. Inst. Phys., Conf. Proc.* **53**, 220-222.

DE WOLFF, P.M., JANSSEN, T. & JANNER, A. (1981): The superspace groups for incommensurate crystal structures with a one-dimensional modulation. *Acta Crystallogr.* **A37**, 625-636.

DUŠEK, M., CHAPUIS, G., MEYER, M. & PETŘÍČEK, V. (2003): Sodium carbonate revisited. *Acta Crystallogr.* **B59**, 337-352.

FERRARIS, G., MAKOVICKY, E. & MERLINO, S. (2004): *Crystallography of Modular Materials*. Oxford University Press, Oxford, U.K.

HARRIS, D.C. & CHEN, T.T. (1976): Crystal chemistry and re-examination of nomenclature of sulfosalts in the aikinite–bismuthinite series. *Can. Mineral.* **14**, 194-205.

HOGERVORST, A., PETERSE, W.J.A.M. & DE WOLFF, P.M. (1979): Modulation wave form for Na_2CO_3. *In* Modulated Structures – 1979 (J.M. Cowley, J.B. Cohen, M.B. Salamon & B.J. Wuensch, eds.). *Am. Inst. Phys., Conf. Proc.* **53**, 217-219.

HORIUCHI, H. & WUENSCH, B.J. (1976): The ordering scheme for metal atoms in the crystal structure of hammarite, $Cu_2Pb_2Bi_4S_9$. *Can. Mineral.* **14**, 536-539.

HORIUCHI, H. & WUENSCH, B.J. (1977): Lindströmite, $Cu_3Pb_3Bi_7S_{15}$: its space group and ordering scheme for metal atoms in the crystal structure. *Can. Mineral.* **15**, 527-535.

KOHATSU, I. & WUENSCH, B.J. (1971): The crystal structure of aikinite, $PbCuBiS_3$. *Acta Crystallogr.* **B27**, 1245-1252.

KOHATSU, I. & WUENSCH, B.J. (1976): The crystal structure of gladite, $PbCuBi_5S_9$, a superstructure intermediate in the series Bi_2S_3–$PbCuBiS_3$ (bismuthinite–aikinite). *Acta Crystallogr.* **B32**, 2401-2409.

MAKOVICKY, E. & MAKOVICKY, M. (1978): Representation of compositions in the bismuthinite–aikinite series. *Can. Mineral.* **16**, 405-409.

MAKOVICKY. E., TOPA, D. & BALIĆ-ŽUNIĆ, T. (2001): The crystal structure of paarite, the newly discovered 56 Å derivative of the bismuthinite–aikinite solid-solution series. *Can. Mineral.* **39**, 1377-1382.

MOZGOVA, N.N., NENASHEVA, S.N., CHISTYAKOVA, N.I., MOGILEVKIN, S.B. & SIVTSOV, A.V. (1990): Compositional fields of minerals in the bismuthinite–aikinite series. *Neues Jahrb. Mineral., Monatsh.*, 35-45.

MUMME, W.G. (1975): The crystal structure of krupkaite, $CuPbBi_3S_6$, from the Juno mine at Tennant Creek, Northern Territory, Australia. *Am. Mineral.* **60**, 300-308.

MUMME, W.G. & WATTS, J.A. (1976): Pekoite, $CuPbBi_{11}S_{18}$, a new member of the bismuthinite–aikinite mineral series: its crystal structure and relationship with naturally- and synthetically-formed members. *Can. Mineral.* **14**, 322-333.

MUMME, W.G., WELIN, E. & WUENSCH, B.J. (1976): Crystal chemistry and proposed nomenclature for sulfosalts intermediate in the system bismuthinite–aikinite (Bi_2S_3–$CuPbBiS_3$). *Am. Mineral.* **61**, 15-20.

OHMASA, M. & NOWACKI, W. (1970a): Note on the space group and on the structure of aikinite derivatives. *Neues Jahrb. Mineral., Monatsh.*, 158-162.

OHMASA, M. & NOWACKI, W. (1970b): A redetermination of the crystal structure of aikinite [$BiS_2|S|Cu^{IV}Pb^{VII}$]. *Z. Kristallogr.* **132**, 71-86.

PETŘÍČEK, V., VAN DER LEE, A. & EVAIN, M. (1995): On the use of crenel functions for occupationally modulated structures. *Acta Crystallogr.* **A51**, 529-535.

PRING, A. (1989): Structural disorder in aikinite and krupkaite. *Am. Mineral.* **74**, 250-255.

PRING, A. (1995): Annealing of synthetic hammarite, $Cu_2Pb_2Bi_4S_9$, and the nature of cation-ordering processes in the bismuthinite–aikinite series. *Am. Mineral.* **80**, 1166-1173.

SYNEČEK, V. & HYBLER, J. (1974): The crystal structure of krupkaite, $CuPbBi_3S_6$, and of gladite, $CuPbBi_5S_9$, and the classification of superstructures in the bismuthinite–aikinite group. *Neues Jahrb. Mineral., Monatsh.*, 541-560.

TOPA, D., BALIĆ-ŽUNIĆ, T. & MAKOVICKY, E. (2000): The crystal structure of $Cu_{1.6}Pb_{1.6}Bi_{6.4}S_{12}$, a new 44.8 Å derivative of the bismuthinite–aikinite solid-solution series. *Can. Mineral.* **38**, 611-616.

TOPA, D., MAKOVICKY, E. & PAAR, W.H. (2002): Composition ranges and exsolution pairs for the members of the bismuthinite–aikinite series from Felbertal, Austria. *Can. Mineral.* **40**, 849-869.

ŽÁK, L. (1980): Isomorphism and polymorphism in the bismuthinite–aikinite group. *Neues Jahrb. Mineral., Monatsh.*, 440-448.

ZUBKOVA, N.V., PUSHCHAROVSKII, D.YU., IVALDI, G., FERRARIS, G., PEKOV, I.V. & CHUKANOV, N.V. (2002): Crystal structure of natrite, γ-Na_2CO_3. *Neues Jahrb. Mineral., Monatsh.*, 85-96.

Received January 19, 2004, revised manuscript accepted October 10, 2005.